

NOAH: User's Manual

Luis Fabián Bonilla^(1,2)

(1) Institute for Crustal Studies, University of California, Santa Barbara, USA

(2) Institut de Radioprotection et de Sûreté Nucléaire, France

1 Introduction

NOAH is a **NO**nlinear **A**nelastic **H**ysteretic finite difference code, which computes the nonlinear wave propagation in water saturated soil deposits subjected to vertically incident SH ground motion. The constitutive equation implemented in this code corresponds to the strain space multishear mechanism model developed by Towhata and Ishihara (1985) and Iai *et al.* (1990). The code is able to perform total and effective stress analyses. The current rheology works particularly well to model the cyclic mobility of sands under undrained conditions. In the following, a simplified summary of the theory implemented in NOAH will be explained. In addition, worked examples will be given so that the user will become familiar with the capabilities of this code.

2 Review of Hysteresis, Pore Pressure, and Wave Propagation Models

The propagation of seismic waves directly depends on the mechanical properties of the material were they travel through. To study and understand the phenomenology of nonlinear soil response to earthquakes, we have developed a numerical model that captures the essential physics of nonlinearity in soils. The model formulation includes nonlinear effects such as anelasticity and hysteretic behavior, and pore pressure generation.

2.1 The Generalized Masing Rules

There have been several attempts to describe the stress-strain space of soil materials subjected to cyclic loads, and among those models the hyperbolic is one of the easiest to use because of its mathematical formulation as well as for the number of parameters necessary to describe it (Hardin and Drnevich, 1972b; Pyke, 1979; Ishihara, 1996; Kramer, 1996; Beresnev and Wen, 1996). In the hyperbolic model, the nonlinear relation is given by the following equation,

$$\frac{G}{G_0} = \frac{1}{1 + \left| \frac{\gamma_{xy}}{\gamma_{ref}} \right|}$$

where $\gamma_{ref} = \tau_0/G_0$ is the reference strain, G_0 is the undisturbed shear modulus, and τ_0 is the maximum shear stress that the material can support in the initial state.

Introducing the equation above into $\tau_{xy} = G\gamma_{xy}$, where τ_{xy} is the shear stress and γ_{xy} is the shear strain; and adding the hysteresis operator, we have

$$\begin{aligned} \tau_{xy} &= Hys(F_{bb}) \\ F_{bb} &= \tau_0 \frac{\frac{\gamma_{xy}}{\gamma_{ref}}}{1 + \left| \frac{\gamma_{xy}}{\gamma_{ref}} \right|} \end{aligned}$$

where F_{bb} is the backbone curve, and $Hys(\cdot)$ is the hysteresis operator (application of the generalized Masing rules). Figure 1 shows the meaning of the symbols describing the model.

Hysteresis behavior can be implemented with the help of the Masing and extended Masing rules (Vucetic, 1990; Kramer, 1996). However, these rules are not enough to constrain the shear stress τ_{xy} to values not exceeding the strength τ_0 . This happens when the time behavior of the shear strain departs from the simple cyclic behavior, and of course, noncyclic time behavior is common in seismic signals. Inadequacy of the Masing rules to describe the

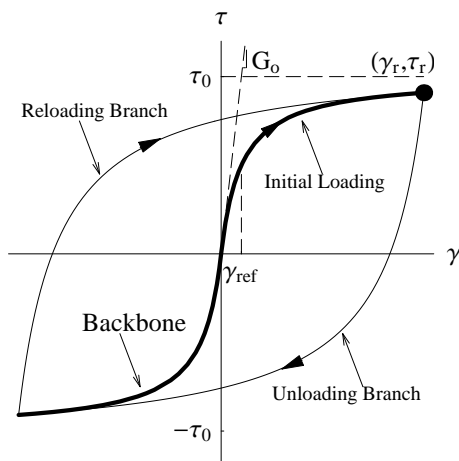


Figure 1: *Hyperbolic model of a stress-strain curve for a soil under cyclic loads. The thick line shows the backbone curve and represents the hyperbolic model. The loading and unloading branches have also the same shape but translated as described by the Masing rules. The slope of the solid straight line is G_0 , and for large strains the stress goes to τ_0 . The pair (γ_r, τ_r) represents the point where the path reverses from loading to unloading.*

hysteretic behavior of complicated signals has been already pointed out and some remedies have been proposed (e.g., Pyke, 1979; Li and Liao, 1993).

The Masing rules consist of a translation and dilatation of the original law governing the strain-stress relationship. While the initial loading of the material is given by the backbone curve $F_{bb}(\gamma_{xy})$, the subsequent loadings and unloadings, the strain-stress relationship is given by:

$$\frac{\tau_{xy} - \tau_r}{\kappa_H} = F_{bb}\left(\frac{\gamma_{xy} - \gamma_r}{\kappa_H}\right)$$

except when the extended Masing rules are applied. The coordinate (γ_r, τ_r) corresponds to the reversal points in the strain-stress space, and κ_H is the so-called hysteresis scale factor (Archuleta *et al.*, 2000). In Masing's original formulation, the hysteresis scale factor κ_H is equal to 2. A first extension to the Masing rules can be obtained by releasing the constrain $\kappa_H = 2$. This parameter controls the shape of the loop in the stress-strain space (Bonilla *et al.*, 1998). However, numerical simulations suggest spurious behavior of

τ_{xy} for irregular loading and unloading processes even when extended Masing rules are used. A further generalization of Masing rules is obtained choosing the value of κ_H in such way to assure that the path τ_{xy} , at a given unloading or reloading, in the strain-stress space will cross the backbone curve, and becomes bounded by the maximum strength of the material τ_0 . This can be achieved by having the following condition,

$$\lim_{\gamma_{xy} \rightarrow \text{sign}(\dot{\gamma}_{xy}) |\gamma_f|} \kappa_{H_j} F_{bb}\left(\frac{\gamma_{xy} - \gamma_{r_j}}{\kappa_{H_j}}\right) \quad |\gamma_{r_j}| \leq |\gamma_f| \leq |\infty|$$

where γ_f is the specified finite or infinite strain condition, γ_{r_j} and κ_{H_j} correspond to the turning point and the hysteresis shape factor at the j th unloading or reloading; and $\text{sign}(\dot{\gamma}_{xy})$ is the sign of the strain rate. Thus,

$$\text{sign}(\dot{\gamma}_{xy}) |\tau_f| = \lim_{\gamma_{xy} \rightarrow \text{sign}(\dot{\gamma}_{xy}) |\gamma_f|} \kappa_{H_j} F_{bb}\left(\frac{\gamma_{xy} - \gamma_{r_j}}{\kappa_{H_j}}\right) + \tau_{r_j}$$

where $|\tau_f| = F_{bb}(|\gamma_f|)$, and $(\gamma_{r_j}, \tau_{r_j})$ is the turning point pair at the j th reversal. Replacing the functional form of the backbone (the hyperbolic model) and after some algebra we have,

$$\kappa_{H_j} = \frac{(\text{sign}(\dot{\gamma}_{xy}) |\tau_f| - \tau_{r_j}) |\text{sign}(\dot{\gamma}_{xy}) |\gamma_f| - \gamma_{r_j}|}{\tau_0 (\text{sign}(\dot{\gamma}_{xy}) |\gamma_f| - \gamma_{r_j}) - \gamma_{ref} (\text{sign}(\dot{\gamma}_{xy}) |\tau_f| - \tau_{r_j})} \quad |\gamma_{r_j}| \leq |\gamma_f| \leq |\infty|$$

The equation above represents a general constraint on the hysteresis scale factor, so that the computed stress does not exceed τ_0 depending on the chosen maximum deformation γ_f that the material is thought to resist. The limit $\gamma_f \rightarrow \infty$ corresponds to the Cundall-Pyke hypothesis (Pyke, 1979), while $\gamma_f = \gamma_{r_j}$ is similar to some extent to a method discussed in (Li and Liao, 1993). The latter formulation presents extended Masing behavior and it is the one implemented in NOAH by default.

An illustration of the behavior of the strain-stress curve is shown in Figure 2 for an irregular loading using the Generalized Masing rules and a backbone curve described by the hyperbolic model.

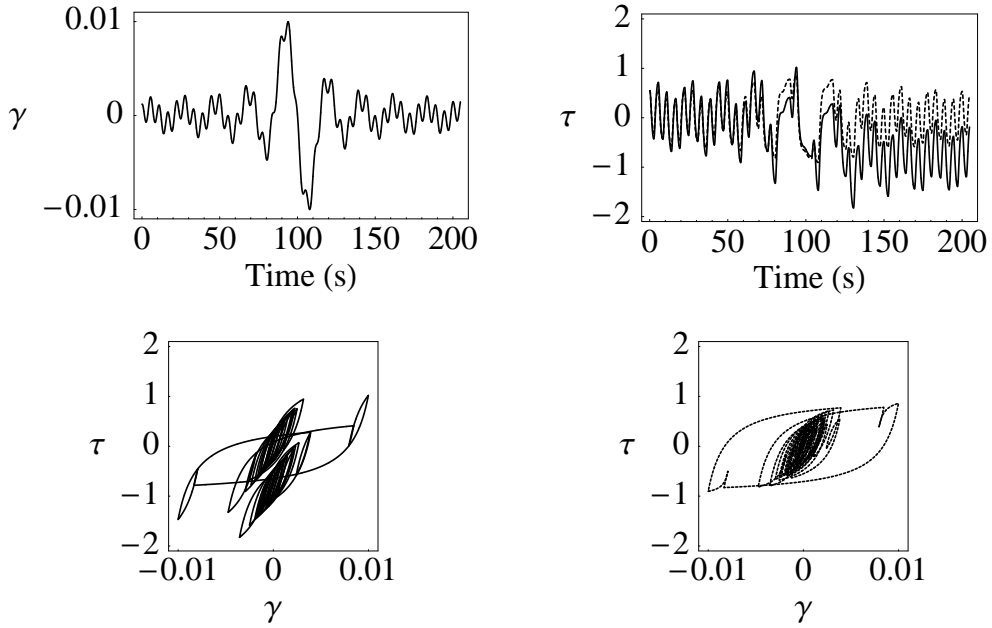


Figure 2: *Example of computed stress time histories following the original Masing rules (solid line), and the model proposed in this study (dash line). Note how the original Masing rule produces that the stress exceeds the maximum strength of the material, in this case 1 kPa.*

Hysteresis Damping of this Model

It has been customary to present the shear modulus reduction and the increasing of damping as function of increasing shear strain as a measure of the material nonlinearity (e.g. Hardin and Drnevich, 1972a). In general, the energy dissipated per cycle ΔW and the damping ratio ξ are related as (Ishihara, 1996; Kramer, 1996)

$$\xi = \frac{\Delta W}{4 \pi W}$$

with the maximum stored energy is given by $W = \gamma_{r_1} F_{bb}(\gamma_{r_j}) / 2$. It is customary to estimate the damping ratio from the first cycle of unloading and reloading. Figure 3 shows the scheme to compute the damping ratio. The energy dissipated per cycle, ΔW , is the area of the loop \widehat{ABCD} ; and the maximum stored energy, W , is the area of the triangle $\widehat{OA}\gamma_r$. The mathematical definition of ΔW consists in integrating $\tau(\gamma)$ over a complete cycle,

$$\Delta W = \int_{-\gamma_{r_1}}^{\gamma_{r_1}} \tau(\gamma) d\gamma$$

which is equivalent to the integration of the first unloading curve from $-\gamma_{r_1}$ to γ_{r_1} added to the integration of the first reloading curve from $-\gamma_{r_1}$ to γ_{r_1} . Where $\pm\gamma_{r_1}$ are the maximum and minimum values of the strain under cyclic loading.

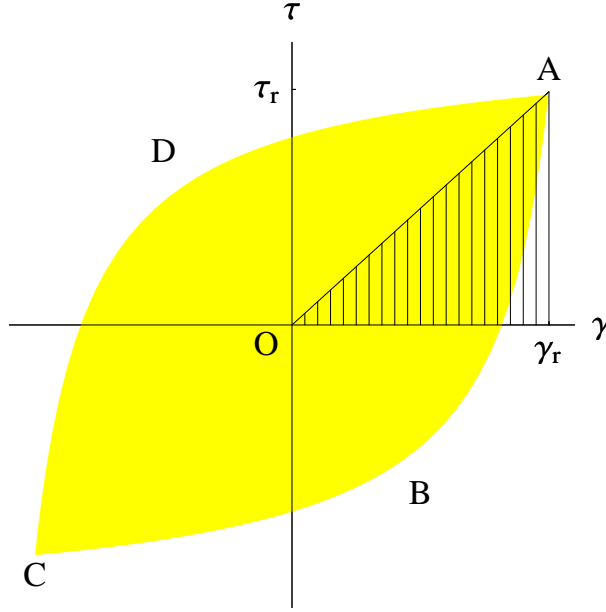


Figure 3: Schematic representation that shows the computation of the damping ratio, ξ , as the ratio of the area of the loop $A\widehat{B}C\widehat{D}$ and 4π times the area of the triangle $O\widehat{A}\widehat{\gamma}_r$.

Using this path integral for ΔW including the hysteresis operator and effective hysteresis scale factor. Furthermore, recalling that the first unloading and first reloading correspond to $j = 1$ and $j = 2$, we have after some simplifications

$$\begin{aligned} \Delta W &= \kappa_{H_2}^2 \int_0^{2\gamma_{r_1}/\kappa_{H_2}} F_{bb}(\gamma') d\gamma' - 2 \gamma_{r_1} \kappa_{H_1} F_{bb}\left(\frac{2\gamma_{r_1}}{\kappa_{H_1}}\right) \\ &\quad + \kappa_{H_1}^2 \int_0^{2\gamma_{r_1}/\kappa_{H_1}} F_{bb}(\gamma') d\gamma' \end{aligned}$$

When the backbone curve is given by the hyperbolic model, the damping ratio ξ becomes

$$\xi = \frac{1}{2\pi} \left(1 + \frac{\gamma_{ref}}{\gamma_{r1}} \right) \left(2(\kappa_{H2} + \kappa_{H1}) - \frac{4}{(\gamma_{ref}/\gamma_{r1}) + (2/\kappa_{H1})} \right) - \left(\frac{\gamma_{ref}}{\gamma_{r1}} \right) \left[\kappa_{H2}^2 \text{Ln} \left(\frac{2\gamma_{r1}}{\kappa_{H2}\gamma_{ref}} + 1 \right) + \kappa_{H1}^2 \text{Ln} \left(\frac{2\gamma_{r1}}{\kappa_{H1}\gamma_{ref}} + 1 \right) \right]$$

where κ_{H1} and κ_{H2} can be obtained from equation that describes the hysteresis scale factor. The equation for ξ provides a relation between the damping and the fiducial point. This expression is complicated since ξ is a transcendental equation of γ_f , and the inverse function $\gamma_f(\xi)$ cannot be easily estimated. However, it can be solved numerically. This means that the damping can be controlled by choosing an appropriate value of γ_f based in experimental data for instance. Finally, this equation reduces to the usual expression of damping ratio when $\kappa_{H1} = \kappa_{H2} = 2$,

$$\xi_M = \frac{2}{\pi} \left[2 \left(\frac{\gamma_{ref}}{\gamma_{r1}} + 1 \right) \left[1 - \left(\frac{\gamma_{ref}}{\gamma_{r1}} \right) \text{Ln} \left(\frac{\gamma_{r1}}{\gamma_{ref}} + 1 \right) \right] - 1 \right]$$

where ξ_M is the damping ratio associated with the Masing rules (Ishihara, 1996).

Damping Control of the Hysteresis Loops

When the hyperbolic model is used, the damping ratio at large deformations is close to $2/\pi$. Experimental data show that maximum damping ratios are between 30% and 40% depending on the material. Ishihara *et al.* (1985) developed a method to control this parameter by recomputing a new backbone curve, which will follow a hysteresis path controlled by the required maximum damping ratio.

Observing the equation for ξ in the previous section, we see that the model depends on the fiducial point γ_{r1} , the reference strain γ_{ref} , and the values of the hysteresis scale factors κ_{H1} and κ_{H2} . If we analyze one complete cycle for a sine strain time history, we can say that $\kappa_{H1} = \kappa_{H2}$. Conversely, the value of the fiducial point is computed depending on the stress reversals; thus, the only 'free' parameter is the reference strain.

What Ishihara *et al.* (1985) did is to recompute the reference strain compatible with the level of deformation γ_{r1} and damping ratio ξ . Once the new reference strain is obtained, a new backbone is computed, which will follow the hysteresis path that obeys a specified damping ratio.

As the reader can see, one may use empirical data for the damping ratio, if available. However, for simplicity we have decided to use an analytical model for the damping suggested by Hardin and Drnevich (1972b),

$$\xi_H = \frac{\gamma_{r1}/\gamma_{ref}}{1.0 + |\gamma_{r1}/\gamma_{ref}|} \xi_{max}$$

where ξ_{max} is the maximum damping that the material may have at large strains. We obtain the new reference strain by equating $\xi = \xi_H$. How does this affect the new backbone curve?

Recall that the original backbone curve is expressed as,

$$\tau_{xy} = \tau_0 \frac{\frac{\gamma_{xy}}{\gamma_{ref}}}{1 + \left| \frac{\gamma_{xy}}{\gamma_{ref}} \right|}$$

this equation can be rewritten as,

$$\tau = \frac{\gamma}{1 + |\gamma|}$$

where $\tau = \tau_{xy}/\tau_0$ and $\gamma = \gamma_{xy}/\gamma_{ref}$. Let a and b be the scaling factors for the stress τ and strain γ , such as $\tau' = \tau/a$ and $\gamma' = \gamma/b$, respectively.

At the first reversal point, the pairs (γ_r, τ_r) and (γ'_r, τ'_r) are the same, this means

$$\tau_r = \frac{\gamma_r}{1 + |\gamma_r|} \quad \text{and} \quad \tau'_r = \frac{\gamma'_r}{1 + |\gamma'_r|}$$

which can be rewritten as,

$$\tau_r = \frac{\gamma_r}{1 + |\gamma_r|} \quad \text{and} \quad \tau_r/a = \frac{\gamma_r/b}{1 + |\gamma_r/b|}$$

solving these two equations for a ,

$$a = \frac{b + |\gamma_r|}{1 + |\gamma_r|}$$

From before, we wish $\xi(\gamma_{r1}/b) = \xi_H(\gamma_{r1})$. The numerical solution (i.e. Newton-Raphson method) of this equation will provide the value of b . Once the scaling factors are computed, the hysteresis operator looks like,

$$\frac{\tau_{xy} - \tau_r}{a\kappa_H} = F_{bb}\left(\frac{\gamma_{xy} - \gamma_r}{b\kappa_H}\right)$$

Figure 4 shows an example of stress-strain loops when original Masing damping is used (left), and when damping control is applied (right). NOAH controls the damping only in layers where no pore pressure is computed.

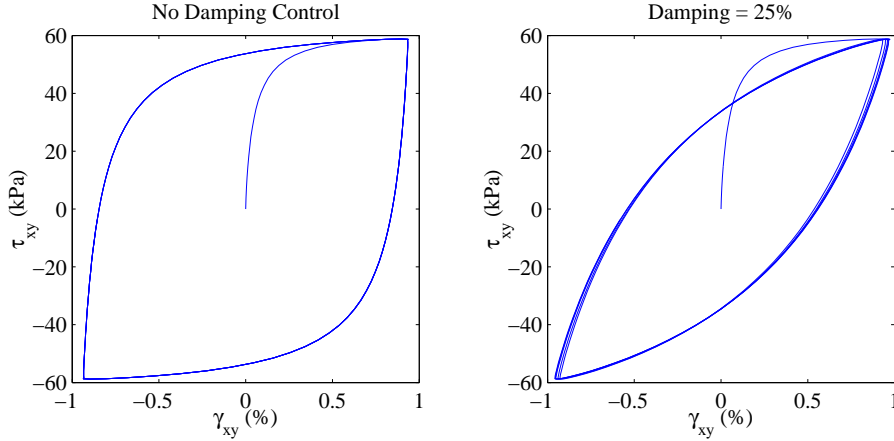


Figure 4: *Example of stress-strain loops showing the effect of controlling the hysteresis damping. On the left, the original Masing rules are used. On the right, the generalized Masing rules with damping control are applied.*

2.2 The Strain Space Multishear Mechanism Model

The multishear mechanism model is a plane strain formulation to simulate cyclic mobility of sands under undrained conditions. This formulation was first implemented by Towhata and Ishihara (1985) to simulate pore pressure generation in sands under cyclic loading and undrained conditions, and further developed by Iai *et al.* (1990a, 1990b) to take into account the cyclic mobility and dilatancy of sands. This method has the following advantages:

- It is relatively easy to implement, it has few parameters, and they can be obtained from simple laboratory tests with pore pressure generation.
- Since the theory is a plane strain condition, it can be developed to study problems in two dimensions, e.g. embankments, quay walls, among others.
- The pore pressure built up is based on the correlation observed in laboratory experiments where it depends on the cumulative shear work done during the shaking mainly.

Model Formulation

The multiple mechanism model relates the effective stress and strain vectors

$$\begin{aligned} [\sigma']^T &= [\sigma'_x \ \sigma'_y \ \tau_{xy}] \\ [\epsilon] ^T &= [\epsilon_x \ \epsilon_y \ \gamma_{xy}] \end{aligned}$$

through the following incremental equation

$$[d\sigma'] = K_a [n^{(0)}] [n^{(0)}]^T ([d\epsilon] - [d\epsilon_p]) + \sum_{i=1}^I R_{L/U}^{(i)} [n^{(i)}] [n^{(i)}]^T [d\epsilon]$$

in which the volumetric strain increment $[d\epsilon_p]$ due to dilatancy is given by

$$[\epsilon_p]^T = [\epsilon_p/2 \ \epsilon_p/2 \ 0]$$

The first term of the incremental equation represents the volumetric mechanism with the associated bulk modulus K_a , and the second part represents the shear mechanism with the tangent shear modulae $R_{L/U}^{(i)}$. The shear mechanism is represented as a collection of multiple springs (the total number is indicated by I), each following the hyperbolic stress-strain model (Figure 5). The shear mechanism is also thought as a combination of pure shear and shear by differential compression. Finally, the subindices L and U indicate the loading and unloading processes, respectively, that follow the generalized Masing rules.

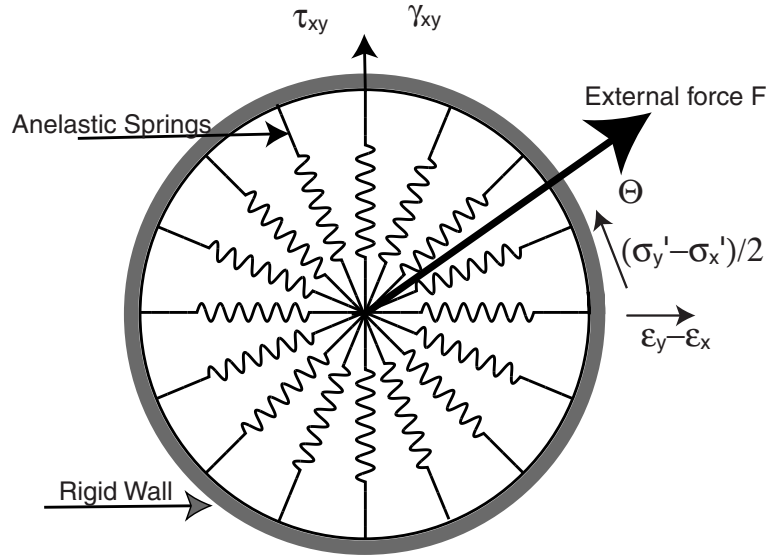


Figure 5: *Schematic figure for the multiple simple shear mechanism. The plane strain is the combination of pure shear and shear by compression (after Towhata and Ishihara, 1985).*

The integrated formulation of the incremental equation is

$$\sigma' = B[(\epsilon_x + \epsilon_y) - \epsilon_p]^2 n^{(0)} + \sum_{i=1}^I Q^{(i)}(\gamma^{(i)}) \Delta \theta n^{(i)}$$

where

$$\begin{aligned}
n^{(0)T} &= [1 \ 1 \ 0] \\
n^{(i)T} &= [\cos \theta_i \ -\cos \theta_i \ \sin \theta_i] \\
\Delta\theta &= \pi/I \\
\theta_i &= (i-1)\Delta\theta
\end{aligned}$$

and

$$\begin{aligned}
B &= [0.5K_a/(\sigma'_{ma})^{0.5}]^2 \\
Q^{(i)}(\gamma^{(i)}) &= [(\gamma^{(i)})/\gamma_v]/(1 + |\gamma^{(i)}/\gamma_v|)Q_v \\
\gamma^{(i)} &= (\epsilon_x - \epsilon_y) \cos \theta_i + \gamma_{xy} \sin \theta_i \\
Q_v &= \tau_0 / \left(\sum_{i=1}^I \sin \theta_i \Delta\theta \right) \\
\gamma_v &= (Q_v/G_0) \left(\sum_{i=1}^I \sin^2 \theta_i \Delta\theta \right)
\end{aligned}$$

here τ_0 is the shear strength, G_0 is the shear modulus, K_a is the bulk modulus, and σ'_{ma} is the reference effective confining pressure. In addition, the volumetric strain produced by the pore pressure ϵ_p is implemented as

$$\epsilon_p = (n/K_f)(\sigma'_{mo} - \sigma'_m) - (\sigma'_m/B)^{0.5} + \epsilon_{\epsilon 0}$$

where n is the porosity, K_f is the bulk modulus of water, σ'_{mo} is the initial effective mean stress, σ'_m is the effective mean stress at any given time (at $t = 0$, $\sigma'_m = \sigma'_{mo}$), and $\epsilon_{\epsilon 0}$ is the initial volumetric strain produced by σ'_{mo} as

$$\epsilon_{\epsilon 0} = (\sigma'_{mo}/B)^{0.5}$$

Initial conditions

The initial effective mean stress σ'_{mo} is computed as

$$\sigma'_{mo} = (\sigma'_{x0} + \sigma'_{y0})/2$$

where

$$\begin{aligned}\sigma'_{y0} &= \rho' g h \\ \sigma'_{x0} &= K_0 \sigma'_{y0}\end{aligned}$$

where ρ' , g , and h are the submerged density, gravity, and depth of the soil element, and K_0 is the coefficient of the earth at rest. The corresponding strains are computed as

$$\epsilon_{e0} = \epsilon_{x0} + \epsilon_{y0}$$

every time that σ'_m is updated, the corresponding strains are computed with the equations above.

Shear Work Correlation and Threshold Limit

Towhata and Ishihara (1985) based on laboratory data (Figure 6) wrote the relationship for the total shear work as

$$dW_{st} = [(\sigma'_x - \sigma'_y)/2]d(\epsilon_x - \epsilon_y) + \tau_{xy}d\gamma_{xy}$$

however, there is a correction to take into account that the pore pressure will not be built up for all strain values (Iai *et al.*, 1990a),

$$\begin{aligned}c_1 dW_{se} &= c_1 |\tau d(\tau/G_m^*)| \\ G_m^* &= G_0 (\sigma'_m/\sigma'_{mo})^{0.5}\end{aligned}$$

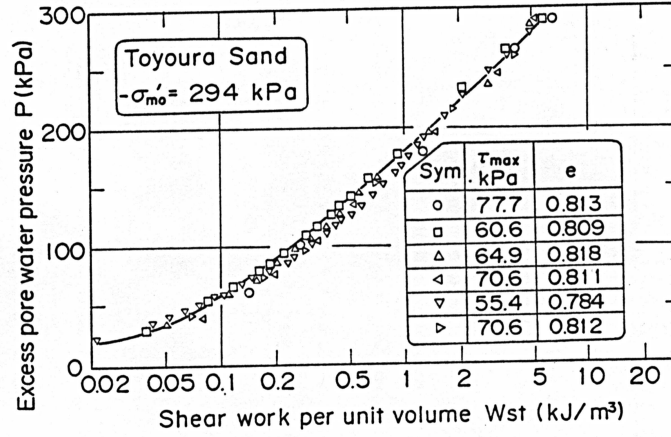


Figure 6: Correlation between the pore pressure build-up and the shear work (after Towhata and Ishihara, 1985).

finally,

$$dW_s = dW_{st} - c_1 dW_{se}$$

where $\tau = (\tau_{xy}^2 + [(\sigma'_x - \sigma'_y)/2]^2)^{0.5}$, which is the total shear stress produced by pure shear and differential stress, and c_1 is a model parameter.

Liquefaction Front

The liquefaction front is an empirical approach to model the decrease of effective mean stress due to the increase of pore pressure (Towhata and Ishihara, 1985; Iai *et al.*, 1990a), see Figure 7. The basis of this assumption is the correlation between pore pressure and shear work found by Towhata and Ishihara (1985). Iai *et al.* (1990a) formulated the liquefaction front concept to simulate the cyclic mobility and dilatancy of sands. The procedure is as follows.

Liquefaction is followed on a shear stress - effective mean normal stress plane, which roughly corresponds to a Mohr-Coulomb plane, Figure 8. During the decrease of the effective mean normal stress, the shear stress approaches the failure line or liquefaction. Here there are two boundaries, one is called

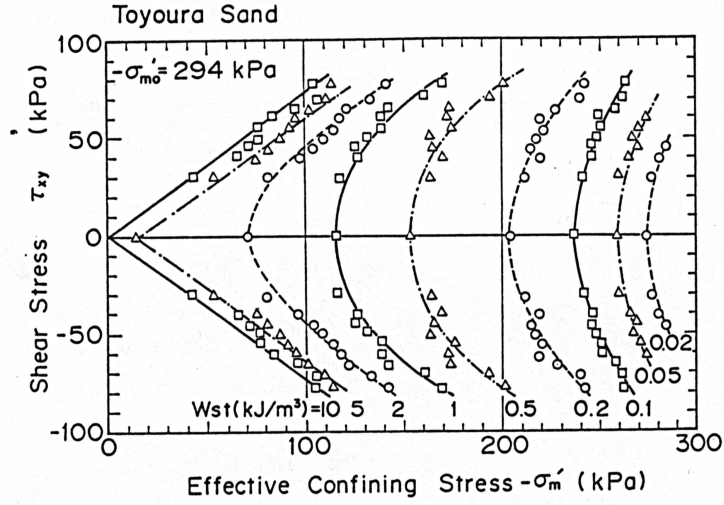


Figure 7: *Effective confining stress decrease as a function of the applied shear stress (after Towhata and Ishihara, 1985). The dash lines correspond to fronts with the same shear work values.*

transformation line (where dilatancy begins), and the other is the failure line (where the liquefaction takes place). These two lines are characterized by the transformation angle ϕ_p , and the friction angle ϕ , respectively.

The liquefaction front is characterized by a state variable S that is the ratio between the current effective mean normal stress σ'_m and the initial effective mean normal stress σ'_{m0} ; it takes values between one (no pore pressure built up) and close to zero (liquefaction). These values are represented by S_0 and are obtained by correlating the plastic shear work with the liquefaction front as,

$$w = W_s/W_n$$

where W_s is the integral of the plastic work defined in the equations above. $W_n = \tau_{m0}\gamma_o/2$ is the plastic work at small strains, and $\gamma_o = \tau_{m0}/G_{m0}$. Iai *et al.* (1990a) used the following empirical relationships to describe the cyclic mobility,

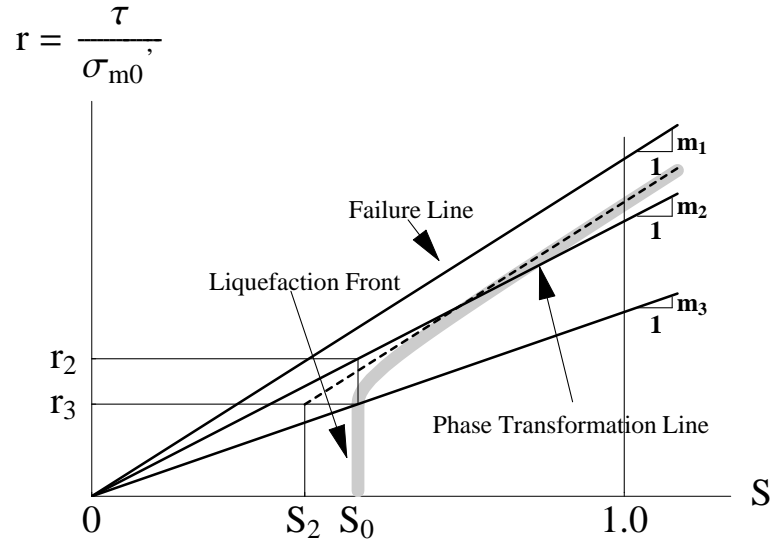


Figure 8: Schematic figure of the liquefaction front, state variable S , and shear stress ratio r (after Iai et al., 1990a).

$$\text{if } w < w_1 \quad S_0 = 1 - 0.6(w/w_1)^{p_1}$$

$$\text{if } w > w_1 \quad S_0 = (0.4 - S_1)(w_1/w)^{p_2} + S_1$$

$$\text{if } r < r_3 \quad S = S_0$$

$$\text{if } r > r_3 \quad S = S_2 + \sqrt{(S_0 - S_2)^2 + [(r - r_3)/m_1]^2}$$

where

$$r_2 = m_2 S_0$$

$$r_3 = m_3 S_0$$

$$S_2 = S_0 - (r_2 - r_3)/m_1$$

$$m_1 = \sin \phi$$

$$m_2 = \sin \phi_p$$

$$m_3 = 0.67m_2$$

where p_1, p_2, w_1, S_1 are the parameters that define the dilatancy of the sands and can be obtained from stress controlled experiments with pore pressure generation. Figure 9 shows the relation between the different parameters. For more details of the model and parameters identification please see Iai *et al.* (1990b).

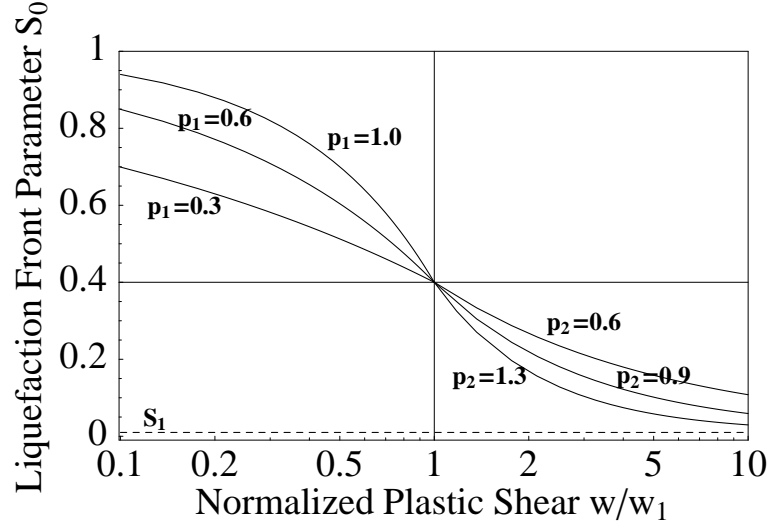


Figure 9: *Dilatancy parameters (after Iai et al., 1990a).*

Further Simplifications

The above formulation as stated corresponds to the two dimensional formulation. However, for the case where infinite horizontal layers, and vertical incident wave propagation is assumed, the problem can be reduced to one dimension. This is easily achieved by constraining the lateral deformation ($\epsilon_x - \epsilon_y$). Thus, the model is driven only by pure shear such as the one produced by the SH vertical incident wave propagation.

2.3 Wave Propagation

In a typical geological setting, the shear wave velocity of the sediments increases with depth. Consequently, seismic wave paths are refracted such that they hit the earth's surface at almost normal incidence. Empirical results also

show that the shear wave dominates the seismic signal. Thus, to a first approximation, the wave propagation can be reduced to a one-dimensional shear wave. The model assumes continuum mechanics and implements a computer-based numerical integration of the one-dimensional shear wave equation of motion,

$$\rho \frac{\partial^2 u}{\partial t^2} = \frac{\partial \tau_{xy}}{\partial y}$$

where u denotes the displacement field perpendicular to the vertical axis at position y and time t , ρ is the density of the material, and τ_{xy} is the shear stress.

The numerical integration of the wave equation is performed using a velocity-displacement-stress staggered grid second order finite difference formulation (Moczo, 1998). The boundary conditions correspond to traction free conditions at surface; and rigid and elastic boundary conditions at the soil-rock interface (Joyner and Chen, 1975). These correspond to,

$$\begin{aligned} \tau_{xy}(y = 0) &= 0 && \text{free surface} \\ \tau_{xy}(y = H) &= \rho_r \beta_r \dot{u} && \text{rigid boundary condition} \\ \tau_{xy}(y = H) &= \rho_r \beta_r (2\dot{u}_+ - \dot{u}_H) && \text{elastic boundary condition} \end{aligned}$$

where ρ_r and β_r are the density and shear wave velocity of the bedrock, \dot{u}_H is the particle velocity at the boundary soil-bedrock, \dot{u}_+ is the particle velocity of the incident wavefield, and H is the depth where the soil-bedrock interface takes place. The nonlinear effective stress code is called hereafter as NOAH.

Stability Conditions

Any numerical solution of the wave equation has to comply with the so-called stability conditions. They are numerical constraints so that the numerical solution is stable (it does not diverge with time) and accurate. The stability conditions are for both discretization grid dy and time step dt ,

$$\begin{aligned} dy &= \frac{V_{min}}{f_{max} ppw} \\ dt &= p_0 \frac{dy}{V_{max}} \end{aligned}$$

where V_{max} and V_{min} are the maximum and minimum velocity of the medium, ppw is the number of points per wavelength, f_{max} is the maximum frequency of the simulation, and p_0 is the fraction of the minimum time step.

Numerical solutions of the linear wave equation uses between 6 to 12 points per wavelength depending on the numerical scheme used. For instance, for a second order scheme the number is 12, and for fourth order scheme the number is 6 (Moczo, 1998). However, in the case of nonlinear wave propagation more points per wavelength are needed to avoid dispersion of the solution.

In nonlinear materials the shear modulus G decreases as the shear strain increases. However, since the shear modulus $G = \rho\beta^2$, a decrease in the modulus reduces the effective shear wave speed, and thus more points per wavelength are needed to make the solution stable. Conversely, the value of p_0 controls the fraction of the time step, so that the numerical solution has the correct phase. Depending on the computed strain, which reflects the shear modulus degradation, the number of points per wavelength should be at least $12\sqrt{10}$.

Implementation of Q

Incorporation of realistic models of intrinsic attenuation in time-domain computations is based on the rheology of the generalized Maxwell body (Day, 1998). The idea is that the stress-strain rheology is modified as

$$\tau_{xy}(t) = G(\gamma_{xy}(t) - \sum_{l=1}^n \zeta_l(t))$$

where G is the shear modulus given by the hyperbolic model, and ζ_l are the memory variables that follow

$$\tau_i \frac{d\zeta_i(t)}{dt} + \zeta_i(t) = \lambda_i \frac{\delta M}{M} \gamma_{xy}(t)$$

where τ_i and λ_i are the relaxation times and quadrature weights that approximate $Q^{-1}(\omega)$ as

$$Q^{-1}(\omega) \sim \frac{\delta M}{M} \sum_{i=1}^n \frac{\lambda_i \omega \tau_i}{\omega^2 \tau_i^2 + 1}$$

The equation above is solved by simulated annealing (P.C. Liu, 2000, Pers. Comm.) to obtain τ_i and λ_i , and $\frac{\delta M}{M}$ is approximated as

$$\frac{\delta M}{M} = 1$$

$Q(\omega)$ in seismology is assumed frequency independent. Its value comes from the damping ratio at low strains ξ , as $Q = 1/(2\xi)$. In general four memory variables are enough to simulate the attenuation in the desired frequency range ($0.1 < f < 20$ Hz) within a 4% accuracy.

3 The Input File

NOAH has an auxiliary code that computes the grid size and time step for the finite difference solution. This code is called PREPNOAH. This code also computes the memory variables used for the approximation of Q . Both codes use the same input file which is organized as follows.

By default, both NOAH and PREPNOAH read the input file that always has the name **input.iai**. This file has three different parts. The first corresponds to the wave propagation variables (e.g. medium size, total time of simulation, etc.). The second part corresponds to the layer information (e.g. velocities, density, Q , etc.). The third part is the boundary condition (e.g. elastic, borehole, or rigid).

For example, let us assume the case of a soil deposit that has two layers. The total thickness of the deposit is 40 m. The first layer has a thickness of 10 m, and the water table is located at 2 m depth. In addition, the ground motion has been recorded at 22 m depth. The rest of information is listed in Table 1.

| Layer | Depth (m) | α (m/s) | β (m/s) | ρ (kg/m ³) | Q | ϕ | K_0 |
|-------|-----------|----------------|---------------|-----------------------------|-----|--------|-------|
| 1 | 0 | 640 | 220 | 1750 | 20 | 35 | 0.5 |
| 2 | 2 | 640 | 220 | 1750 | 20 | 40 | 0.5 |
| 3 | 10 | 1500 | 350 | 1850 | 50 | 40 | 0.5 |
| Rock | 22 | 1500 | 350 | 1850 | | | |

Table 1: *Material properties model for the example downhole array.*

Note that the computational model has three layers instead of two. This is because the first layer has been divided in two sublayers. The first is dry, and the second contains the water table. This is because even in the case of total stress analysis, NOAH will compute the effective vertical stress if the water table is present. This will affect the maximum strength of the layer. Another observation is on what is called rock in Table 1. This is actually the same layer No. 3. This is because the second layer has a thickness of 30 m, but the ground motion was recorded at 22 m depth. Thus, the boundary condition is borehole, and there is no impedance contrast.

A short comment on the boundary conditions. If the user has total motion data, that means the recorded waveform at depth is from borehole sensors, the boundary condition is borehole. This boundary condition is useful when the recorded motion is deep and there is no way of separating the total wavefield from the incident wavefield.

Conversely, the elastic or transmitting boundary conditions are more natural to use. However, that means that the wavefield should be the incident wavefield. The computation of the incoming wavefield is left to the user with his/her method. The user should only be aware that if he/she decides to use

the elastic boundary condition, the assumption of incident wavefield is made.

Finally, the incident wavefield cannot easily be computed from surface records when strong nonlinearity has taken place. In such cases, if down-hole records are available, use them as borehole boundary conditions for the nonlinear computation.

Having said that, the **input.iai** file looks like:

```
10.      freqmax
22       ppw
0.01    p0
22.     medsize
40.     duration
2.      water table
1.E-2   dt0
15.     flowp
0.1     fhigh
BP      (HP=high pass, LP=low pass, BP=bandpass)
5.0     rpos
3       nlayers
##### layer 1: #####
0.      top
640.    Vp
220.    Vs
1750.   density
1.0E-5  (0 = linear, nonlinear otherwise)
20.     Q
0.0 0.0E3 0.0E3  viscosity, sigma_ma, cohesion
0.0     porosity
0.5     Ko
35.     phi
0.      pha
0.      p1
0.      p2
0.      w1
0.      S1
0.      c1
0.3     Hmax
##### layer 2: #####
2.      top
640.    Vp
220.    Vs
1750.   density
```

```

1.0E-5      (0 = linear, nonlinear otherwise)
20.         Q
0.0 0.0E3 0.0E3  viscosity, sigma_ma, cohesion
0.45        porosity
0.5         Ko
40.         phi
28.         pha
0.5         p1
0.65        p2
7.0         w1
0.01        S1
3.97        c1
0.3         Hmax
##### layer 3: #####
10.         top
1500.       Vp
350.        Vs
1850.       density
1.0E-5      (0 = linear, nonlinear otherwise)
50.         Q
0.0 0.0E3 0.0E3  viscosity, sigma_ma, cohesion
0.          porosity
0.5         Ko
40.         phi
0.          pha
0.          p1
0.          p2
0.          w1
0.          S1
0.          c1
0.3         Hmax
##### bedrock: #####
350.        velocity
1850.       density
borehole    (borehole, elastic, rigid)

```

The values in **input.iai** are self explanatory and are related to the equations described in the previous sections. Note that all values follow the MKS metric system. However, the input and output acceleration time histories are given in cm/s/s just because that is customary in seismology. Yet, additional detail is needed for the following parameters.

- If the P-wave velocity is unknown, set a zero value. NOAH will assume a poisson ratio of 0.33 to compute the P-wave speed from the shear wave velocity.
- NOAH in practice uses a viscosity term in order to control the high frequency damping during the wave propagation (Bardet and Tobita, 2001). The addition of the viscosity term helps to assure numerical stability. Its value, η is chosen following the formulation proposed by Li (1990) as,

$$\eta = \frac{C_0 G_0}{\pi f_0}$$

where C_0 is the fraction of viscous damping, usually around 0.01, and f_0 is the minimum frequency of the signal to be damped, usually between 1 and 5 Hz. NOAH uses by default $f_0 = 1$ Hz. C_0 is what is called viscosity in **input.iai**.

- The field σ_{ma} is the so-called effective reference stress (Iai *et al.*, 1990a). This stress is basically the effective confining stress at the middle of each layer. If a negative value is used, the effective confining pressure is automatically computed by the code. If the user wishes a specific value it has to be a positive one. The use of this parameter is to correct the values of the shear and rebound modulae as a function of depth as follows:

$$G = G_0 \left(\frac{\sigma'_{mo}}{\sigma'_{ma}} \right)^{0.5}$$

$$K = K_a \left(\frac{\sigma'_{mo}}{\sigma'_{ma}} \right)^{0.5}$$

NOAH has implemented this option; however, if the user does not want to perform this correction, put 0.0 in the corresponding field. This is the

case used in the example. The units of the effective confining pressure are in Pascals.

- When clayey soils are modeled, they need the cohesion (in Pascals) in order to compute the maximum shear strength as

$$\tau_{max} = coh \cos(\phi) + \sigma'_{m0} \sin(\phi)$$

- The porosity n is obtained from laboratory data. If $n \leq 0$, the excess of pore pressure is not computed. The porosity is related to the void ratio e as

$$n = \frac{e}{1 + e}$$

- The coefficient of earth at rest K_0 may be computed as function of the angle of the internal friction ϕ and the overconsolidation ratio OCR ,

$$K_0 = (1 - \sin \phi)OCR^{\sin \phi}$$

- The remaining parameters, except for the angle of internal friction ϕ , can be ignored if no excess of pore pressure is computed ($n \leq 0$). If the pore pressure is computed, then the dilatancy parameters, $\phi_p, p_1, p_2, w_1, S_1, c_1$ need to be specified.
- The final field H_{max} is the maximum damping value at large strains for total stress analysis only. When pore pressure is computed this field is not used. It is a dummy value. This value can be obtained from the damping curves coming from the laboratory. For clays H_{max} is between 20% to 25%, and for sands between 30% to 40%, respectively.

4 Determination of the Dilatancy Parameters

The dilatancy parameters are values that describe the dynamic behavior of a dilatant material. In what follows we will see how to determine those parameters from modeling simple cyclic shear stress in a soil element using the multishear mechanism.

The dilatancy parameters can be determined in two different ways. Both ways are complementary; however, they can be used independently as well. The first is when stress controlled experiment data are available. The second corresponds to the fit of the liquefaction strength curve. Most of the time, only the latter is available from the laboratory experiments. Note, however, that the liquefaction strength is obtained from stress controlled experiments.

- The first parameter is the transformation phase angle ϕ_p (variable **pha** in **input.iai**). This corresponds to the angle that divides the contractive from the dilative zone. It defines the phase transformation line in Figure 8. If no laboratory data are available, $\tan(\phi_p) = \frac{5}{8}\tan(\phi)$ can be assumed (Ishihara and Towhata, 1982).
- In the following, a transcript from Iai *et al.* (1990b) is shown. First of all, the test data, commonly available in the practice of soil dynamics, should be provided for representing (i) a liquefaction resistance curve (i.e. the cyclic shear stress ratio vs. the number of the cyclic loading N_1 required to cause shear strain of 5% in double amplitude), (ii) an envelope of an excess pore water pressure generation curve such as shown in Figure 10 by a broken line, and (iii) and envelope of shear strain amplitude such as shown in Figure 11 by broken lines.
- The parameter S_1 takes small positive value of about 0.005 so that S_0 will never be zero. In such a special case as the stress strain curve should become a closed loop during the cyclic mobility, S_1 can take a larger value and can be determined in a trial and error manner.

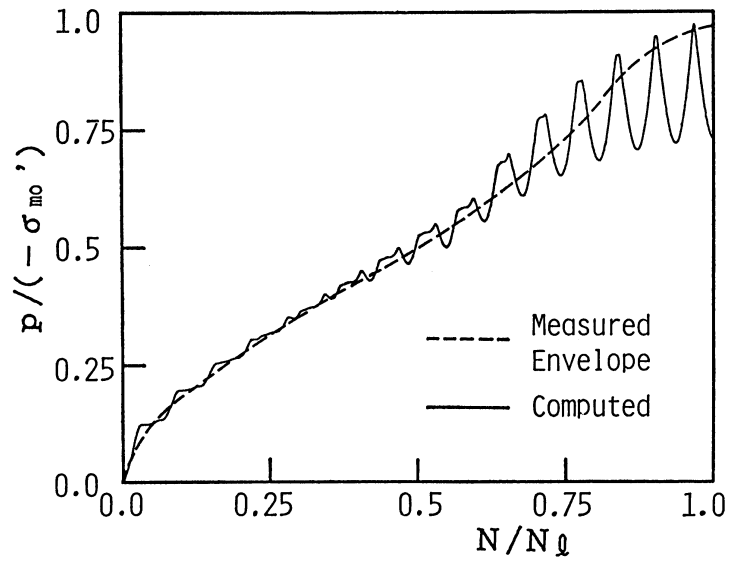


Figure 10: *Excess pore water pressure generation curve (after Iai et al., 1990b).*

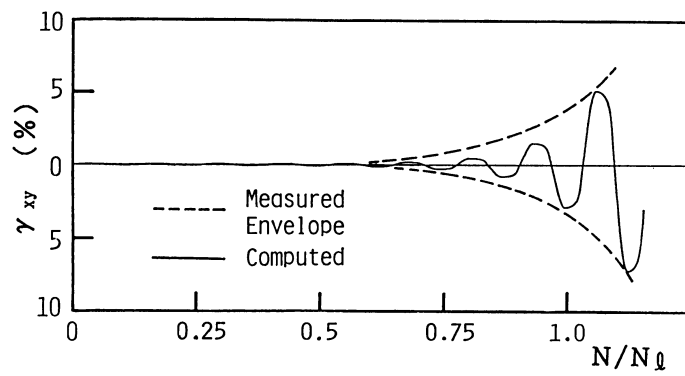


Figure 11: *Shear strain amplitude (after Iai et al., 1990b).*

- The parameter c_1 for specifying the threshold level is temporarily fixed to 1.0 as the first guess. The value of c_1 will later be modified in a trial and error manner. The modification in the value of c_1 , however, does not have a great influence upon the cyclic mobility when the shear stress ratio is much higher than the threshold level. Therefore, with $c_1 = 1.0$, the rest of the parameters w_1, p_1, p_2 are determined by the following steps from the test results with a relatively large shear stress ratio.
- The parameters w_1 and p_1 are determined in a trial and error manner from the excess pore water pressure generation curve. In particular, the portion of the curve for $p/(-\sigma'_{m0}) < 0.6$ is used, in which p denotes excess pore water pressure. Because w_1 is not significantly influenced by variation in p_1 , the parameter w_1 is at first determined with an appropriate guess of p_1 . The value of p_1 ranges from 0.4 to 0.7. With the determined value of w_1 , the value of p_1 is determined. In general the greater w_1 is, and the greater p_1 is, the more slowly the pore water pressure rises.
- Though the parameter p_2 could also be determined from the pore water pressure generation curve for $p/(-\sigma'_{m0}) > 0.6$, it is better to determine this parameter from the envelope of strain amplitude if the primary purpose of the cyclic mobility analysis is to estimate the amount of deformation in soil structures and foundations. The value of p_2 ranges from about 0.6 to 1.5; the greater p_2 is, the faster the shear strain amplitude increases.
- When all the parameters are determined by the steps mentioned above from the laboratory data with a relatively large shear stress ratio, the next step is to examine if these parameters are also appropriate for representing the laboratory data at a relatively small shear stress ratio.

If not, then the parameter c_1 is modified in a trial and error manner. With increasing c_1 , the higher threshold level is achieved.

5 Compiling and Running NOAH

Once the input file has been completed PREPNOAH is ready to be used. First PREPNOAH has to be compiled. It is a one time compilation. This code outputs the time step, grid size, and memory values for computing Q . These parameters in term are used to determine the size of the arrays in NOAH. The ouput of PREPNOAH are the files: intermed.par and Q.par.

The user also should be aware that NOAH's input and output acceleration time histories are in SAC format. There is also a postprocessor program W2LAB, which will be explained in the corresponding section that uses MATLAB libraries. Thus, the user should contact his/her system administrator to know about the details of those programs (SAC and MATLAB) before compiling NOAH's codes.

The following is a simple makefile that can be used and modified to compile NOAH's codes. The compilation instructions and paths are optimized for my Linux box.

```
# makefile for compiling NOAH's programs

F77=f77 # FORTRAN 77
F90=f90 # FORTRAN 90

FAST_FLAG = -O3
SACLIB = /home/fabian/Tools/SAC2000/lib # SAC library
MATLIB = /usr/local/matlab6/extern/lib/glnx86 # MATLAB library
LDSAC = -L${SACLIB} -L/usr/X11R6/lib
LDMAT = -L${MATLIB}
LIBS = -lsac -lnsl -lX11
LIBM = -lmat -lmx -lmi -lut -lnsl

all: prepnoah noah w2lab stress2strain

clean:
```

```
/usr/bin/rm -f core *.o *% *stress* *strain* *water*
```

```
prepnoah : prepnoah.f90  
${F90} ${FAST_FLAG} -o $@ $@.f90
```

```
noah : noah.f90  
${F90} ${FAST_FLAG} ${LDSAC} -o $@ $@.f90 ${LIBS}
```

```
w2lab : w2lab.f  
${F77} ${FAST_FLAG} ${LDMAT} -o $@ $@.f ${LIBM}
```

```
stress2strain : stress2strain.f90  
${F90} ${FAST_FLAG} -o $@ $@.f90
```

this makefile uses the F90 compiler **f90**. Thus, first compile PREPNOAH and NOAH, and then run them as follows:

```
make prepnoah noah
```

```
prepnoah y
```

where **y** says to PREPNOAH to compute the memory variables for Q . The output of PREPNOAH are the files: `intermed.par`, and `Q.par`. They look like:

- **intermed.par:**

```
          23    nx  
        1408652  nt  
        2.8396E-05 dt  
        9.9386E-01 dx  
             1   iskix
```

- **Q.par:**

```
0.00688002724  0.148935959  0.292529911  
0.0488630421  0.00867180619  0.211700663  
0.281062007  -0.0197941065  0.20329462  
1.85879183   -0.13781397   0.292474926  
0.    0.236348256  
2.    0.236348256  
10.   0.102340549
```

If the user decides to change the points per wavelength or p_0 , the Q values do not need to be recomputed, thus PREPNOAH can be called as:

```
prepnoah n
```

NOAH can now be used as:

```
noah input.sac output.sac
```

where **input.sac** and **output.sac** are the file names of the input and the computed acceleration time histories in SAC format, respectively. NOAH will also output the following files: **output.strain.sac**, **output.stress.sac**, and **output.water.sac**. They are the shear strain, shear stress, and excess of pore water pressure (if computed) time histories at the desired depth. In addition, NOAH flushes in real time an ASCII file called **output.dat**, which contains the velocity, strain, stress, and effective mean stress at the same dt_0 time step of the input time history. This file can be used in MATLAB, SCILAB, or MATHEMATICA to observe the evolution of the computations.

For example, if the user has MATLAB installed, NOAH comes with a MATLAB script, DIB2B, that reads **output.dat** and plots the current computed values as shown in Figure 12.

6 Postprocessing

NOAH also outputs a binary file that contains the velocity, strain, stress, and water pore pressure every $kipx \times dx$ meters. Its name is **Nwavefield** and it has all those data multiplexed. The postprocessor code W2LAB demultiplexes this file, and dumps the corresponding files in MATLAB format. Two MATLAB scripts, MAXST and DIBT, read those files and plot the distribution of maximum strain versus depth, and snapshots as the one shown in Figure 12 at the different depths. The user can use his/her imagination to plot the results as wished.

In Linux, the FORTRAN 90 version of W2LAB works fine with the MATLAB libraries; this is not the case for the UNIX version of MATLAB. Thus,

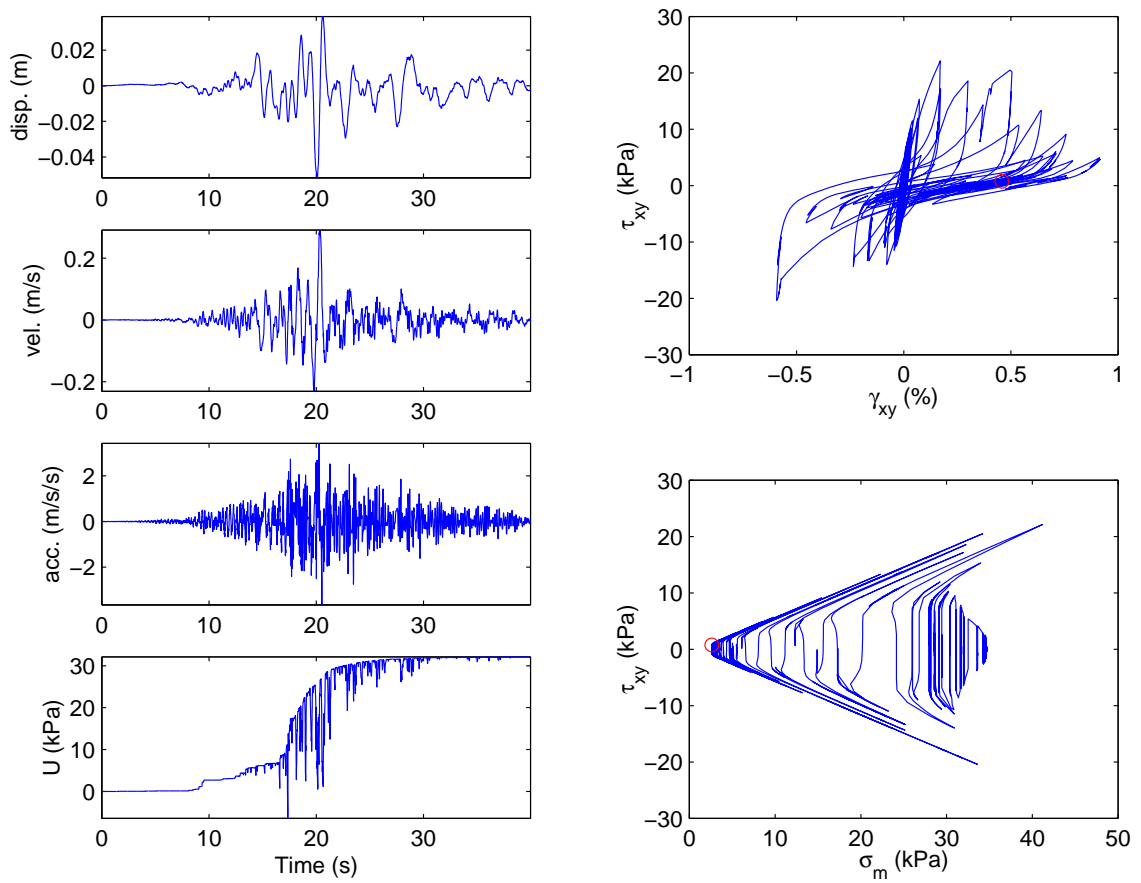


Figure 12: Computed acceleration, velocity, displacement time histories, and the corresponding stress-strain loop, stress path, and excess of pore pressure at GL-5m.

W2LAB is written in FORTRAN 77 and it has to be compiled every time that the user changes the number of nodes in the 1D grid. The user may write:

```
make w2lab
```

```
w2lab Nwavefield
```

the output files of W2LAB are: velocity.mat, stress.mat, strain.mat, and meanstress.mat.

Appendix: Determination of the Dilatancy Parameters

We have already seen how to determine the dilatancy parameters in the previous sections. In the following we will stress the procedure using a code called STRESS2STRAIN. This program simulates simple shear laboratory experiments under stress controlled conditions. It uses the same rheology as NOAH; however, the numerical solution is made solving the equilibrium equations at each time step (quasi-static conditions). One observation, STRESS2STRAIN uses a Newton-Raphson method with line searches to solve the nonlinear equations. The method is implemented in a very simple way (the line searches algorithm). As a consequence the code is quite slow. The user may modify this program as he/she wishes, and send us a copy of a faster version.

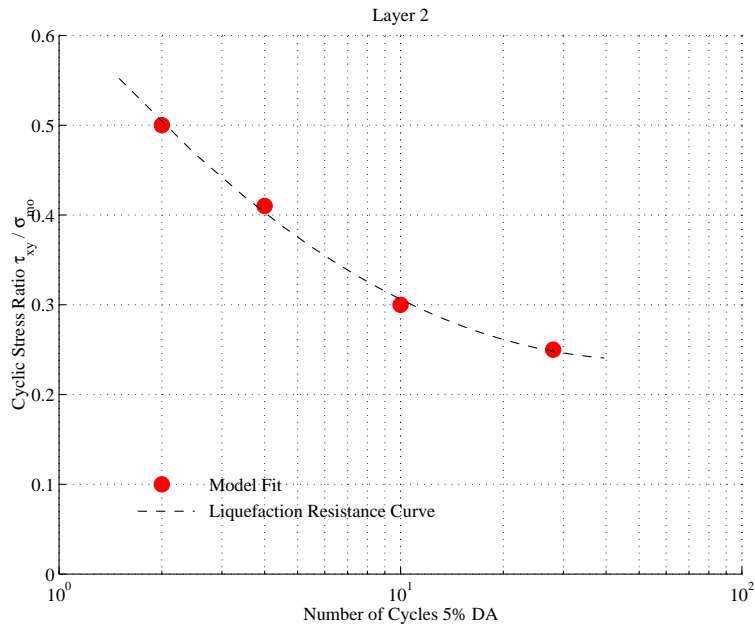


Figure 13: *Liquefaction resistance curve for the second layer listed in Table 1. The laboratory data are represented by the dashed line, and the fit to the model by the solid circles.*

As an example we will try to obtain the dilatancy parameters that model the liquefaction resistance curve shown in Figure 13.

Modifying the amplitude cyclic stress ratio, we proceed to seek for the

dilatancy parameters that best model Figure 13 by a trial and error manner. An example of the **output** file from STRESS2STRAIN is shown in Figure 14. STRESS2STRAIN is called as:

stress2strain inputfile

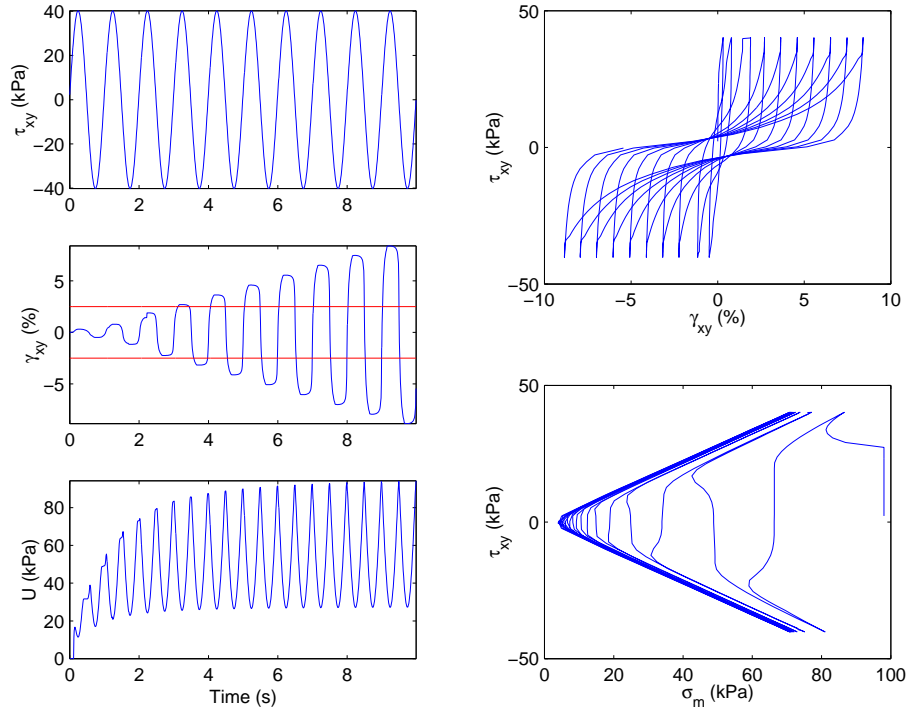


Figure 14: *Synthetic stress controlled experiment when the cyclic stress ratio is 0.41. The effective confining stress here is 98 kPa. The straight lines in the strain time history represent the 5% double amplitude threshold. In this case $N = 4$.*

The input file, **kl2.inp**, looks like:

```
isine.dat      strainfile
0.41          cyclic stress ratio
1.0E-2        dt
10           Ncycles
12           IM
0.45         poro
2.2E9        Kf
640.0        Alpha (m/s)
220.0        Beta (m/s)
40.0         phi
28.0         pha
```

| | |
|--------|--------------------------|
| 0.5 | p1 |
| 0.65 | p2 |
| 7.0 | w1 |
| 0.01 | S1 |
| 3.97 | c1 |
| 1750.0 | rho (kg/m ³) |
| 1.0 | Ko |
| 10.0 | depth (m) |
| 0.0E3 | sigma_ma (kPa) |
| 98.0E3 | sigma_confining (kPa) |
| 0.3 | Hmax |

the file that plots Figure 14 is called DIBONE.M. The final dilatancy parameters are listed in Table 2.

| Layer | w_1 | p_1 | p_2 | c_1 | S_1 |
|-------|-------|-------|-------|-------|-------|
| 2 | 7.0 | 0.5 | 0.65 | 3.97 | 0.01 |

Table 2: *Dilatancy parameters for Layer 2.*

References

- Archuleta, R.J., L.F., Bonilla, and D. Lavallée (2000). Nonlinearity in observed and computed accelerograms. Proceedings of the 12th World Conference on Earthquake Engineering, published by Aston Koedyk Ltd., Paper reference number 0338.
- Beresnev, I.A., and K.L. Wen (1996). Nonlinear Site Response - A Reality? *Bull. Seism. Soc. Am.*, **86**, 1964-1978.
- Bonilla, L. F., Lavallée, D. and Archuleta, R. J. (1998), Nonlinear site response: Laboratory modeling as a constraint for modeling accelerograms, Proceeding of the Second International Symposium on the Effects of Surface Geology on Seismic Motion, Vol. 2, edited by K. Irikura, K. Kudo H. Okada and T. Sasatani, A.A. Balkema: Netherlands, 793-800.
- Hardin, B.O., and V.P. Drnevich (1972a). Shear modulus and damping in soil: measurement and parameter effects, *J. Soil Mech. Foundations Div. ASCE*, **98**, 603-624.
- Hardin, B.O., and V.P. Drnevich (1972b). Shear modulus and damping in soil: design equations and curves, *J. Soil Mech. Foundations Div. ASCE*, **98**, 667-692.
- Iai, S., Y. Matsunaga, and T. Kameoka (1990a). Strain Space Plasticity Model for Cyclic Mobility, *Report of the Port and Harbour Research Institute*, **29**, 27-56.
- Iai, S., Y. Matsunaga, and T. Kameoka (1990b). Parameter Identification for Cyclic Mobility Model, *Report of the Port and Harbour Research Institute*, **29**, 57-83.
- Ishihara, K., and I., Towhata (1982). Dynamic response analysis of level ground based on the effective stress method, in Soil Mechanics - Transient and Cyclic Loads, G.N. Pande and O.C. Zienkiewicz Eds., 133-172.
- Ishihara, K. (1996). Soil Behaviour in Earthquake Geotechnics, Clarenton Press, Oxford, 350 pp.

- Ishihara, K., N. Yoshida, and S. Tsujino (1985). Modelling of stress-strain relations of soils in cyclic loading, *Fifth International Conference on Numerical Methods in Geomechanics*, Nagoya, 373-380.
- Joyner, W., and A.T. Chen (1975). Calculation of Nonlinear Ground Response in Earthquakes, *Bull. Seism. Soc. Am.*, **65**, 1315-1336.
- Kramer, S.L. (1996). Geotechnical Earthquake Engineering, Prentice Hall, New Jersey, 653 pp.
- Li, X., (1990). Free field response under multidirectional earthquake loading, Ph.D. dissertation, University of California, Davis.
- Li, X., and Z. Liao (1993). Dynamic skeleton curve of soil stress-strain relation under irregular cyclic loading Earthquake research in China, **7**, 469-477.
- Moczo, P. (1998). Introduction to Modeling Seismic Wave Propagation by the Finite Difference Method, Lecture notes given at the Disaster Prevention Research Institute, Kyoto University.
- Masing, G., (1926). Eigenspannungen und Verfertigung beim Messing, *Proceedings, 2nd International Congress on Applied Mechanics*, Zurich.
- Pyke, R. (1979). Nonlinear soil model for irregular cyclic loadings. *J. of the Geotech. Engrg. Div.*, **105**, 715-726.
- Towhata, I., and K. Ishihara (1985). Modeling Soil Behavior Under Principal Axes Rotation, *Fifth International Conference on Numerical Methods in Geomechanics*, Nagoya, 523-530.
- Vucetic, M. (1990). Normalized behavior of clay under irregular cyclic loading, *Can. Geotech. J.*, **27**, 29-46.